American Mineralogist, Volume 88, pages 996–1002, 2003

Bulk moduli and high-pressure crystal structures of minium, Pb_3O_4, determined by X-ray powder diffraction

ROBERT E. DINNEBIER,[1] STEFAN CARLSON,[2] MICHAEL HANFLAND,[3] AND MARTIN JANSEN[1,*]

[1] Max-Planck-Institute for Solid State Research, Heisenbergstrasse 1, D-70569 Stuttgart, Germany
[2] MAX-lab, Lund University, P.O. Box 118, SE-22100 Lund, Sweden
[3] Experiments Division High Pressure Group, European Synchrotron Radiation Facility, B.P. 220, F-38043 Grenoble CEDEX, France

ABSTRACT

We report the pressure dependence of the crystal structure of lead tetroxide ($p \leq 41.05$ GPa, $T = 298$ K) using high-resolution angle-dispersive X-ray powder diffraction. Pb_3O_4 shows two reversible phase transitions in the measured pressure range. The crystal structures of the modifications identified have in common frameworks of $Pb^{+4}O_6$ octahedra and irregular $Pb^{+2}O_{4+1}$ respectively $Pb^{2+}O_{6+1}$ polyhedra. At ambient conditions, Pb_3O_4 crystallizes in space group $P4_2/mbc$ (phase I). Between 0.11 and 0.3 GPa it exhibits a displacive second order phase transition to a structure with space group *Pbam* (phase II). A second displacive phase transition occurs between 5.54 and 6.6 GPa to another structure with space group *Pbam* (phase III) but halved *c* dimension. A non-linear compression behavior over the entire pressure range is observed, which can be described by two Vinet relations in the ranges from 0.28 to 5.54 GPa and from 6.6 to 41.05 GPa. The extrapolated bulk moduli of the high-pressure phases were determined to be $K_0 = 21(2)$ GPa for phase II and $K_0 = 91(3)$ GPa for phase III. The crystal structures of all phases were refined from X-ray diffraction powder data collected at several pressures between 0.06 and 41.05 GPa. Except for their cell dimensions, phases I and II were found to be isostructural to the corresponding phases at low temperatures, whereas phase III can be derived from the Sr_2PbO_4 aristotype. With increasing pressure, the lone pair which is localized at Pb^{2+} adopts increasingly pure *s*-character, which is reflected by the similar coordination polyhedra of Pb^{2+} in Pb_3O_4 (phase III) and of Sr^{2+} in Sr_2PbO_4.

INTRODUCTION

In chemical compounds exhibiting significant covalent bonding contributions, "lone", i.e., non-bonding, electron pairs can be strongly stereochemically active. Generally they are regarded as pseudo-ligands that are able to replace one or more of the regular ligands in a given coordination sphere. The resulting stereochemical implications have been discussed in depth (Gillespie 1967; Gillespie and Robinson 1996), and the model derived has also been applied to extended solids (Brown 1974; Galy et al. 1975). In parallel to the strong geometric effects, the physical properties are also affected. The anisotropic local environments of those atoms bearing a "lone-pair" in their valence shells frequently induce the formation of acentric or even polar crystal structures, leading to known consequences for the dielectric properties (Avanesyan et al. 2002).

Since the structures formed are rather open, and moreover cations with "lone-pairs" exhibit high polarizabilities, such compounds showing lone-pair related structural features should be highly susceptible to pressure-induced phase transitions. Geometric and electronic structures of solids are strongly correlated. Thus, with transformation to a reorganized structure of higher density one would expect significant changes in the electronic structure. Several different scenarios can be imagined: (1) the "lone-pair" could be forced into a pure *s*-type state, removing all anisotropies in the coordination sphere; (2) the valence band, in most instances also including the non-bonding electron pair, (Terpstra et al. 1997) and the conduction band will broaden or even overlap, leading to semiconducting or metallic behavior, respectively; (3) in mixed valence representatives the originally localized lone-pair might delocalize, making the valence states of the respective metal ions indiscernible (Robin and Day 1970) and producing a partially filled band at the Fermi level, again leading to metallic behavior. The latter situation has attracted attention recently, in the context of trying to understand superconductivity observed to occur in oxides containing metal ions featuring "lone-pairs" (Anderson 1975; Robaszkiewicz et al. 1987; Simon 1987, 1997; Micnas et al. 1990). The theoretical models nourish prospects for being able to induce superconductivity in such compounds by applying high external pressures. In the context of the above considerations the mixed valence lead tetroxide Pb_3O_4 appears to be a good candidate for probing such an approach.

Lead tetroxide, also known as "red lead" or minium (named after the Minius River in northwest Spain) is an oxidation product of lead minerals (mainly galenite). Although the Latin term minium was used in general for the red pigment used in painting, the word became fixed on the lead oxide in the seventeenth century. It is interesting to note that the word miniature for small paintings in old manuscripts has its origin in the italian

* E-mail: m.jansen@fkf.mpg.de

0003-004X/03/0007–996$05.00

word miniare, to illuminate, which itself comes from the Latin minire, to color red. Minium forms at extreme oxidizing conditions from lead ore bodies and its presence is very indicative for the degree of oxidation, making it of special interest to petrologists. It commonly exists as a slight reddish coating on many lead specimens. Artificially produced minium is still used as a pigment in corrosion-resistant paints and dyes despite the health hazard. Minium also finds industrial applications in lead oxide pastes for tubular lead-acid batteries, in ballistic modifiers for high-energy propellants, in ceramic glazes for porcelain, in lubricants for hot pressing metals, in radiation-shielding foam coatings in clinical X-ray exposures, and in rubber adhesives for roadway joints (Ullmann 2002 and references therein).

Minium is considered a member of the spinel group of oxide minerals, although the crystal structures are quite different. In minium, the lead atoms occur in two different valence states, $(Pb^{+4})(Pb^{+2})_2O_4$, where the free electron pair of Pb^{+2} can be considered as an additional ligand, causing severe distortions of the coordination polyhedra. Minium is a semiconductor with a band gap of 2.1(1) eV; this has been confirmed experimentally (reflectance and photovoltaic technique) and theoretically (augmented spherical wave method) (Terpstra et al. 1997 and references therein).

The crystal structure of minium at room temperature with space group $P4_2/mbc$ was first determined by Bystroem and Westgren (1943). Upon cooling a displacive phase transition at 270 K to an orthorhombic phase (space group *Pbam*) was discovered by Gavarri and Weigel (1975). The thermal behavior of minium between room temperature and 5K was studied by Gavarri et al. (1978). They also found that upon heating, minium undergoes two additional ferroelectric respectively, ferroelastic displacive phase transitions from *Pbam* to non-centrosymmetric orthorhombic, at 195 K to non-centrosymmetric tetragonal, and finally at 225 K to $P4_2/mbc$.

In this work, we have investigated the pressure dependence of the crystal structure of Pb_3O_4 which we consider a prerequisite for future investigations of the transport properties of Pb_3O_4 under lasting pressure or possible quenched high-pressure modifications. For this purpose, in situ X-ray powder diffraction measurements were performed at room temperature and elevated pressures using a diamond anvil cell (DAC).

EXPERIMENTAL METHODS

X-ray diffraction measurements

Our sample of Pb_3O_4 was prepared following the recipe given by Brauer (1978).

For the X-ray powder diffraction experiments, the sample was placed in two membrane driven diamond-anvil cells (DAC) (Letoullec et al. 1988), one with silicon oil, the other with nitrogen (cryogenic loading) as pressure mediums. The DAC with silicon oil as the pressure medium was equipped with 500 μm diameter diamonds and a stainless steel gasket with a 250 μm diameter hole, while the DAC using nitrogen as the pressure medium had 300 μm culets and a 125 μm hole. Pressure was determined by the ruby luminescence method using the wavelength shift calibration of Mao et al. (1986). High pressure X-ray powder diffraction data were collected at room temperature at beamline ID9 of the European Synchrotron Radiation Facility (ESRF). Monochromatic radiation for the high-pressure experiment was selected at 29.8 keV (0.41594 Å). A (111) channel-cut Si monochromator, operated in vacuum (water-cooled), was irradiated by synchrotron radiation from a standard undulator with a 46 mm period. The X-rays were focussed vertically by a Pt-coated Si mirror and horizontally by an asymmetrically cut bent Si(111) monochromator (Schulze et al. 1998). The beam size was 30 × 30 μm. Diffracted intensities were recorded with a Marresearch Mar345 online image plate system. A set of eight images (silicon oil as the pressure medium) at selected pressures between 0.06 and 2.12 GPa and a second set of 33 images (nitrogen as the pressure medium) at selected pressures between 1.5 and 41.05 GPa were recorded. Exposure times were between 10 and 30 seconds. Data reduction was performed using the program FIT2D (Hammersley et al. 1996), resulting in diagrams of corrected intensities vs. the scattering angle 2θ (Fig. 1). We observed that the diffracted intensity was quite uniformly distributed over the Debye-Scherrer rings, ruling out severe grain size effects and preferred orientation. All data sets could be indexed with ITO (Visser 1969). Further experimental details are given in Table 1.

Crystal structure determination and refinement

The dependence of the scattering profile on pressure gave evidence for two second order phase transitions (Fig. 1). The phase with tetragonal symmetry ($P4_2/mbc$) (phase I), which is stable at ambient conditions, is retained up to at least 0.11 GPa. A transition to a phase with orthorhombic symmetry (*Pbam*) (phase II) was observed between 0.11 and 0.3 GPa, and is stable to at least 5.54 GPa. Between 5.54 and 6.58 GPa a second phase transition occured to another orthorhombic phase (*Pbam*; halved *c* dimension) (phase III) which stayed stable until at least 41.05 GPa (Fig. 2). Thus, an interesting sub-super group relation has been found with increasing pressure starting from $p\frac{4_2}{m}bc$ to the maximal non isomorphic *subgroup Pbam* and finally to the mineral isomorphic supergroup of the latter *Pbam* (index 2). For all data sets, lattice parameters as a function of pressure were obtained with Le Bail-type fits using the programs FULLPROF (Rodríguez-Carvajal 2001) and GSAS (Larson and VonDreele 1994); these are available as supplemental material. Backgrounds were modeled manually using the program GUFI (Dinnebier 1993). Peak-profiles were described by a pseudo-Voigt function in combination with a special function that accounts for the asymmetry due to axial divergence (Thompson et al. 1987; Finger et al. 1994). The powder patterns of phase I exhibit severe anisotropic peak broadening caused by lattice strain with the sharpest peaks along the face diagonals of the **a-b** plane, and along the **c**-direction having a minimum full-width at half-maximum (FWHM) of 0.06° 2θ and the broadest peaks along the tetragonal **a** direction with a peak width of about 0.3° 2θ. The phenomenological strain model of Stephens (1999) as implemented in GSAS was used to model the anisotropy of the FWHM. Four parameters were refined for the tetragonal phase. A three dimensional representation of the isosurface of the microstrain of phase I is shown in Figure 3. The anisotropic lattice strain decreases rapidly with increasing pressure for the higher pressure phases II and III. Significant isotropic line broadening of the diffraction maxima caused by non-hydrostatic conditions was observed for pressures above 30 GPa. The quality of the powder

TABLE 1. Lattice parameters and details of refinement of Pb_3O_4 at 13.3 GPa (phase III)

Pressure (GPa)	13.3
a (Å)	9.3812(3)
b (Å)	6.4610(3)
c (Å)	3.3168(1)
V(Å^3)	201.04(1)
V/Z(Å^3)	100.52
Z	2
Space group	*Pbam*
ρ_{calc} (g/cm^3)	11.166
Formula weight	675.92
μ(cm^{-1})	294.81
Temperature (K)	295
R_p (%)	2.5
R_{wp} (%)	3.8
R_F (%)	5.4
R_{F^2} (%)	9.3
No. of reflections	127
No. of variables	27
No. of refined atoms	4
Wavelength (Å)	0.41594
2θ range (°), counting time (s)	3.6–23.8, 20
Step size (° 2θ) (after rebinning)	0.01

Notes: R_p, R_{wp}, R_F, and R_{F^2} refer to the Rietveld criteria of fit for profile, weighted profile, and structure factor, respectively, defined in Langford and Louër (1996).

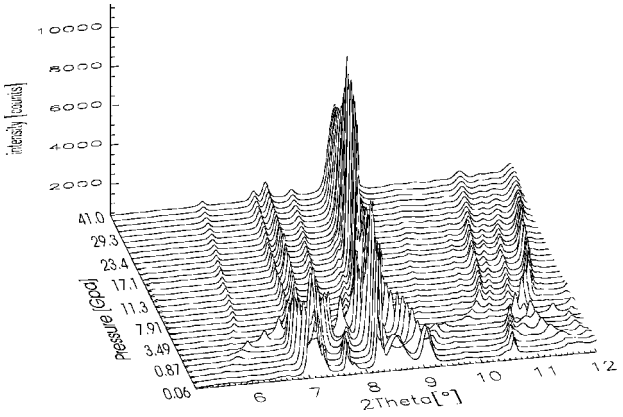

FIGURE 1. Scattered X-ray intensity of Pb_3O_4 as a function of diffraction angle 2θ and pressure (non linear pressure scale from 0.06 GPa to 41.05 GPa). The wavelength was 0.41594 Å. Phases identified are in order of increasing pressure: $P4_2/mbc$ ($0 < P \leq 0.12$ GPa), *Pbam* ($0.3 \leq P \leq 5.54$ GPa), *Pbam* ($c' = c/2$) ($6.59 \leq P \leq 41.05$ GPa).

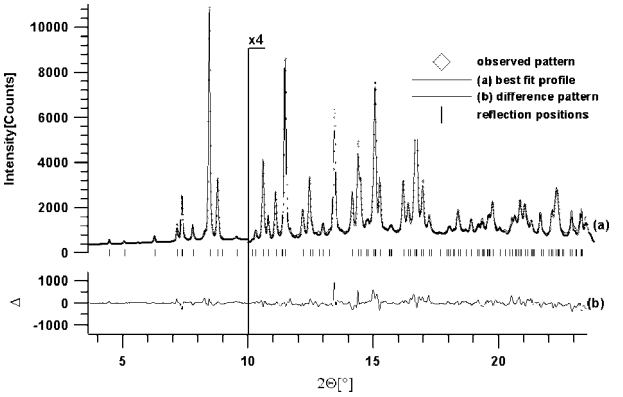

FIGURE 2. Scattered X-ray intensity for the high pressure phase III of Pb_3O_4 at P = 13.3 GPa as a function of diffraction angle 2θ. Shown are the observed pattern (diamonds), the best Rietveld fit profile in *Pbam* (line a), the difference curve between observed and calculated profile (line b), and the reflection markers (vertical bars). The wavelength was 0.41594 Å. The higher angle part starting at 10.0° 2θ is enlarged by a factor of four.

patterns of phases I and II was sufficient to extract lattice parameters and to verify the crystal structures via Rietveld refinement. All powder patterns of phase III contained sufficiently resolved diffraction peaks to allow for ab initio crystal structure determination as well as for Rietveld refinement. The direct methods program EXPO (Altomare et al. 1999) was used to determine the positions of the two crystallographically independent lead atoms. Subsequent Rietveld refinements in combination with difference-Fourier analysis then revealed the positions of the two O atoms in the asymmetric unit. For the Rietveld refinements using the program GSAS, the lattice and reflection profile parameters were first kept at the values as obtained from the LeBail fits. Slack soft constraints for the four Pb^{+4}-O bond lengths of 2.2(1) Å were used to stabilize the refinements of the crystal structure of phase III. Unconstrained refinements led to small but meaningless distortions of the almost regular octahedron without improving the weighted profile *R*-factor (R_{wp}). The final R_{wp} converged to values close to that of the best Le Bail fits (Fig. 2).

RESULTS AND DISCUSSION

X-ray scattering of Pb_3O_4 at various pressures provided lattice parameters as a function of pressure. From these results, the pressure dependence of the relative volume was derived (Fig. 4). Whereas *V* decreases at most by 0.6% with temperature (Gavarri et al. 1978), it decreases by 32% at 41 GPa, indicating a very soft and highly compressible material. The volume/pressure relation represents the equation of state (EoS), which can be described analytically by series expansions of Eulerian finite strain (Birch-Murnaghan EoS) or cohesive energies in a condensed system (Vinet EoS). The data for phases II (nine data points) and III (21 data points) could be adequately fitted to several widely used EoS using the program EOSFIT 5.2 (Angel 2002). The best results were obtained with the Vinet EoS (Vinet et al. 1986), which is believed to yield more accurate parameters for highly compressible materials than the Birch-Murnahgam EoS (Angel 2000). The Vinet EoS is defined as

$$P = 3K_0 \frac{(1-f_v)}{f_v^2} \exp\left(\frac{3}{2}\left(K' - 1\right)\left(1 - f_v\right)\right),$$

where

$$f_v = \left(\frac{V}{V_0}\right)^{1/3}$$

with volume at zero pressure V_0, the bulk modulus K_0, and its pressure derivative at zero pressure and ambient temperature *K′*. The results are given in Table 2. Two dashed lines drawn through the volume data in Figure 4 represent the fitted Vinet EoS. The small jumps in the lattice parameters as a function of pressure for phase III (at approximately 13 GPa) are due to overnight relaxation of the DAC and the instrument. The bulk modulus of phase II in comparison to the corresponding values of phase III is about 4.7 times lower indicating a much higher compressibility. This behavior can be related to packing effects of the Pb^{2+} polyhedra at low pressure due to a change in space requirements of the free electron pair. According to a

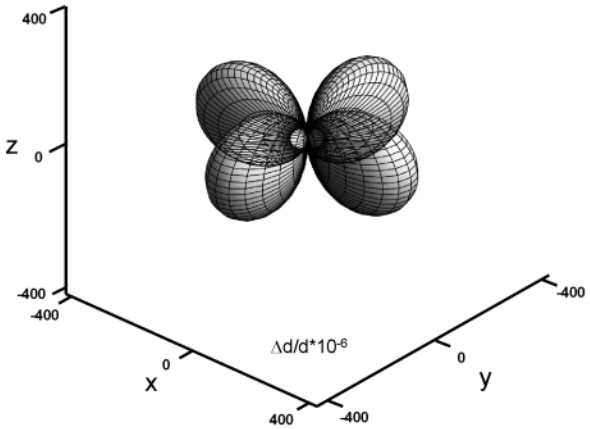

FIGURE 3. Isosurface of the anisotropic microstrain of the tetragonal phase of Pb_3O_4 at 0.06 GPa.

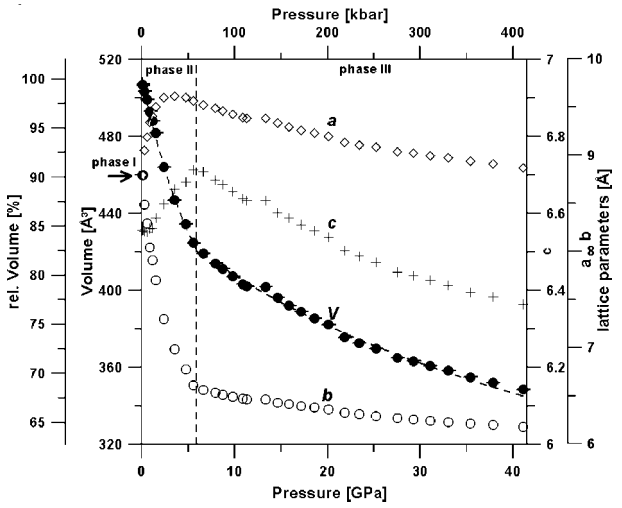

FIGURE 4. Dependence of the lattice parameters, volume, and relative volume of Pb_3O_4 on pressure in the range 0-41.05 GPa. The high pressure phase transition between the two orthorhombic phases (II, III) at approximately 6 GPa is marked by a vertical dashed line. For better comparison, the c axis of phase III is doubled. The dashed fitted lines correspond to least squares fits of Vinet equations of state for the two orthorhombic phases (II, III).

hard sphere model, the space filling at ambient conditions (phase I) is only 44.2%, which is far away from a closed packed structure, and it increases rapidly until the stable high pressure phase III (60% at 13.3 GPa) is obtained. The pressure dependence of the lattice parameters shows a distinct anisotropy, which reflects the space requirements of the free electron pair of Pb^{2+}. Lattice parameter *b* decreases rapidly (–0.4 Å/GPa) with increasing pressure with an abrupt decrease in slope at the phase II/III border (–0.01 Å/GPa). The *c* parameter first increases with increasing pressure (0.03 Å/GPa) with an abrupt sign change at the phase II/III border (–0.01 Å/GPa). Lattice parameter *a* increases rapidly (0.4 Å/GPa) with increasing pressure up to about 3GPa, stays stable until 5 GPa, and then decreases slowly (–0.02 Å/GPa). In general, an almost uniform decrease of *a*, *b*, and *c* with increasing pressure up to 41 GPa is observed for phase III. This observation is in accordance with the observed anisotropic microstrain. Since microstrain is directly related to the elasticity of the material, it is obvious from Figure 3 that the compressibility along the **a**-axis is much higher as compared to the **c**-axis, indicating that any major pressure-induced changes in the crystal structure of minium are likely to occur along the **a**- and **b**-axes. Literature values of calculated bulk moduli for Pb_3O_4 and similar compounds with lone pairs (Gavarri 1982; Chater et al. 1987; Gavarri and Chater 1989) are in good agreement with the average value of the compressibility of phases II and III of Pb_3O_4 (59.4 GPa) (Table 2).

The temperature dependence in the temperature range from room temperature down to 30 K (Gavarri et al. 1978) shows an almost linear decrease of the volume of –0.01 Å³/°. The lattice parameter *c* decreases at a rate of -4×10^{-5} Å/° until the phase I/II border at 170 K before it starts increasing at the same rate. The tetragonal *a*-parameter decreases linearly by -5×10^{-5} Å/°

TABLE 2. Parameters of the Vinet equation of state for the two high pressure phases of Pb_3O_4 and literature values of the bulk moduli of Pb_3O_4 and related compounds

Vinet EoS	V_0 (Å)	K_0 (GPa)	K'	R_w (%)
Pb_3O_4 (phase II)	511(1)	20.8(4)	4 (fix)	3.65
Pb_3O_4 (phase III)	222(2)	98(3)	4 (fix)	4.25
Pb_3O_4		67(16) *		
$SnSb_2O_4$		49(8) *		
$NiSb_2O_4$		57 ‡, 65(5) †		
$ZnSb_2O_4$		52(9) *		
$MnSb_2O_4$		55 ‡		
$FeSb_2O_4$		50 ‡		

* Gavarri (1982) (calculated values).
† Chater et al. (1987) (measured at T = 63 K and T = 240 K).
‡ Gavarri and Chater (1989) (calculated values).

until the phase I/II barrier after which an parabolic split into *a*– (negative slope) and *b*– (positive slope) parameters occurs. Gavarri and Weigel (1982) proposed an algebraic expression for the dependence of the cell parameters of the orthorhombic phase II of Pb_3O_4 with temperature, demonstrating the blocking role of the lone pairs with decreasing temperature.

From the Rietveld refinements of the powder patterns of phases I and II at high pressure it can be concluded that they are isostructural with their counterparts at low temperature. In particular the high quality of the powder patterns of the previously unknown phase III of minium permitted high quality Rietveld refinements and therefore allowed the accurate determination of structural parameters with pressure (Fig. 2).

Crystal structures of phases I and II

The crystal structure of the tetragonal phase I at ambient conditions consists of infinite chains of distorted $Pb^{4+}O_6$ octahedra with a twist angle in the base plane of almost 20° (Fig. 5a). Within the chain, the polyhedra are connected via common edges of their base planes. Each chain of octahedra is surrounded by four neighboring chains which are rotated by 90° with respect to the central chain, corresponding to an expanded rutile structure. All Pb^{2+} ions are located in the planes spanned by the shared edges of neighboring chains of octahedra, thus forming bridges between the chains which run in a zigzag manner along the **c**-axis. The Pb^{2+} ions are coordinated by four O atoms forming an irregular $Pb^{2+}O_4$ pyramid with the four O atoms forming the non-planar base and the lead atoms sitting at the vertex. Three of the coordinating O atoms belong to the same chain; the fourth one belongs to the neighboring chain of octahedra. The free electron pair of the Pb^{2+} ion points along the face diagonal of the **a-b** plane, opposite the four coordinating O atoms, thus forming large channels in the structure which explains the low space filling at ambient conditions of only 44.2%. The empty channel is thus comprised of a stack of edge sharing Pb^{2+}-tetragonal bisphenoids ($\bar{4}$) with Pb^{2+}-Pb^{2+} distances of 3.79 Å and 4.24 Å. The phase transitions can be attributed to small changes of the orientation of the lone pairs of the highly polarizable Pb^{2+} ions. Thus, the crystal structure of the orthorhombic phase II can be directly derived from the tetragonal phase I by anisotropic compression of the empty channels. A splitting of the Pb^{2+} sites occurs, turning the Pb^{2+}-tetragonal

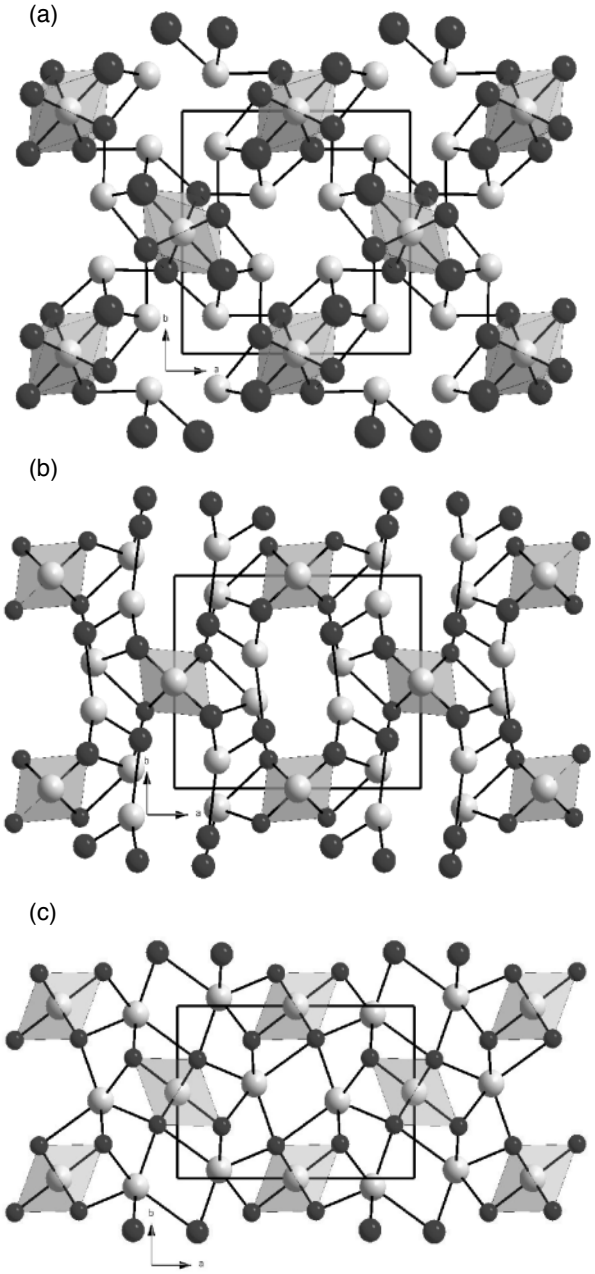

FIGURE 5. Ball and stick model of the crystal structure of Pb_3O_4 at 0.1 Gpa (phase I) (**a**), at 1.5 Gpa (phase II) (**b**), and at 13.3 GPa (phase III) (**c**) in a projection along the c axis. The $Pb^{+4}O_6$ octahedra are shown.

bisphenoids into orthorhombic bisphenoids (222). Furthermore, the twist angle within the $Pb^{4+}O_6$ octahedra disappears leading to a more regular octahedron.

Crystal structure of phase III

The basic crystal packing of phases I/II (Figs. 5a and 5b) is preserved in phase III (Fig. 5c, Table 3). Phase III forms when the external pressure is strong enough to flatten the Pb^{2+}- orthorhombic bisphenoids to rectangular sheets, making the two different Pb^{2+} sites crystallographically indistinguishable again, leading to an unexpected increase of symmetry at higher pressure. The main difference of the crystal structure of minium at pressures above 6.58 GPa is the increase of the coordination number of Pb^{2+} from 4 to 6+1, forming distorted $Pb^{2+}O_7$ trigonal prisms with a pyramidal vertex on one of the rectangular planes (Fig. 6). Each $Pb^{2+}O_7$ polyhedron is connected via two triangular faces of the trigonal prism with two mirrored $Pb^{2+}O_7$ polyhedra along **b**, thus forming infinite chains. These chains are interconnected with neighboring chains along **c** via two common edges of the base plane of the trigonal prism, thus forming infinite two-dimensional puckered sheets perpendicular to **a**. The regular $Pb^{4+}O_6$ octahedra form infinite chains running along **c**, interconnecting consecutive layers of $Pb^{2+}O_7$ polyhedra. Each $Pb^{2+}O_7$ polyhedron shares two pyramidal edges with two consecutive $Pb^{4+}O_6$ octahedra. In addition, the roof edges of the trigonal prisms of neighboring layers are also shared, completing the framework structure. The packing may be viewed as a strongly distorted hexagonal closed packing (hcp) arrangement leading to the formula $(Pb^{+4}\square_3)^{VI}(Pb^{+2}_{2}\square_6)^{IV}O_4$ (Fig. 7). The resulting crystal structure is of Sr_2PbO_4 aristotype. Table 4 compares geometrical data between phase III of Pb_3O_4 at P = 13.3 GPa, phase I of Pb_3O_4 at ambient conditions (Gavarri and Weigel 1975), $Pb^{2+}O$ (Garnier et al. 1990), $Pb^{+4}O_2$ (Harada et al. 1981), and Sr_2PbO_4 (Trömel 1969). Small differences between the crystal structures of Pb_2PbO_4 (phase III) and Sr_2PbO_4 arise in different distortions of the $Pb^{2+}O_7$ respectively. $Sr^{2+}O_7$ polyhedra due to sterical requirements of the lone pair of lead (II). Whereas the long metal-O atom bond in the $Sr^{2+}O_7$ polyhedron connects the O atom at the pyramidal vertex with the central cation (2.99 Å), there is an O atom at the roof of the trigonal prism in the case of the $Pb^{2+}O_7$ polyhedron (2.95 Å) (Fig. 6). The small deviations of the central cations from the centers of gravity of the capped trigonal prism are basically identical (0.25–0.3 Å) for both compounds. This structural relationship clearly indicates that the stereochemical needs of

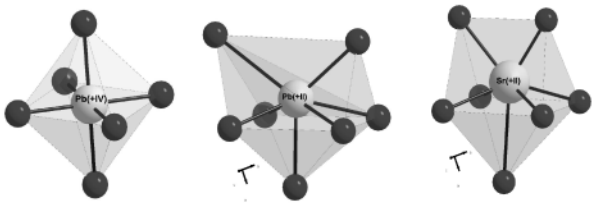

FIGURE 6. Regular $Pb^{+4}O_6$ octahedron (**left**) and irregular $Pb^{+2}O_{6+1}$ capped trigonal prism (**middle**) in Pb_3O_4 at 13.3 GPa (phase III) and the $Sr^{+2}O_{6+1}$ capped trigonal prism in Sr_3PbO_4 at ambient conditions (**right**).

TABLE 3. Positional parameters and u_i/Å^2 ×10^2 of phase III of Pb_3O_4 at 13.3 GPa

	x/*a*	*y*/*b*	*z*/*c*	u_i
Pb1	0.67564(17)	0.94970(32)	0.5	1.4(2)
Pb2	0.5	0.5	0	1.7(3)
O1	0.3132(29)	0.3014(34)	0	4.2(7)
O2	0.5841(23)	0.3108(22)	0.5	4.2(7)

Note: The Rietveld statistical estimates are given in parenthesis. The values of the temperature factor are constrained to be equal for the two O atoms.

Pb^{2+} under high pressure are similar to those of Sr^{2+}. Thus the response of the electronic structure to external pressure follows scenario (1), as outlined in the introduction, and the lone pair has adopted an almost pure *s*-type, which is further supported by the similarity of the $Sr^{2+}O_{6+1}$ and $Pb^{2+}O_{6+1}$ coordination polyhedra. Also, the somewhat global approach for estimating the degree of stereochemical activity of lone electron pairs as suggested by Galy et al. (1975) gives strong support for our view that the stereochemical activity of the lone pair at Pb^{2+} is virtually gone in the high pressure modification of minium (Table 4). The packing density calculated by MAPLE (Hübenthal 1991) further supports this idea. The packing density of Pb_3O_4 (phase I) is close to that of β-$Pb^{2+}O$ (41%) due to the sterical requirements of the lone pairs. However, the packing densities for β-$Pb^{4+}O_2$, Sr_2PbO_4, and Pb_3O_4 (phase III at 13.3 GPa) are typical for close-packed structures, and show no signs of stereoactive lone pairs.

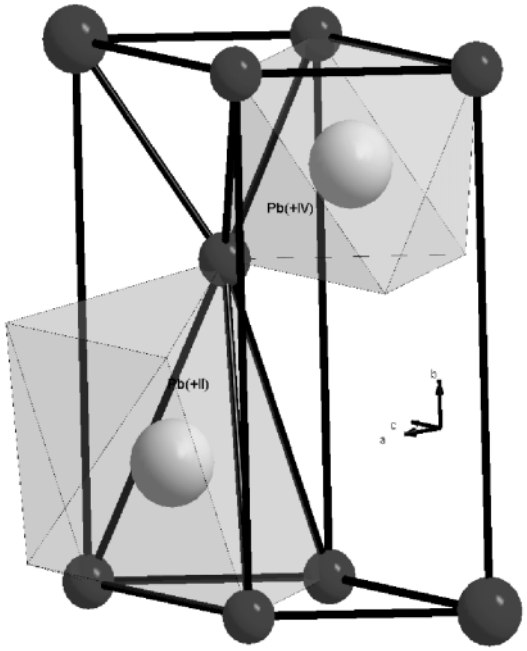

FIGURE 7. Hexagonal closed packing (hcp) arrangement of Pb_3O_4 at 13.3 GPa leading to the formula $(Pb^{+4}\square_3)^{VI}(Pb^{+2}_2\square_6)^{IV}O_4$.

It is interesting to note, that of the more than 3000 crystal structures of general type $M1M2M2_2X4$ found in the ICSD database (2001 edition), about 20 substances adopt the type of crystal structure found for the high pressure modification of Pb_3O_4 (phase III), among which is, for example, the high pressure modification of Mn_2GeO_4 that belongs to the olivine group (Wadsley et al. 1968, Morimoto et al. 1972). Wadsley et al. derived a dependency of the structure type on the unit-cell volume vs. the two median metal-oxygen distances that also fits for phase III of minimum. Based on this work, the same structuure type has been theoretically proposed as a stable candidate for olivine at very high pressures (Baur 1972) but has not been observed yet.

ACKNOWLEDGMENTS

We are grateful to A. Aruraj (University of Bayreuth) for his kind assistance with the measurements. Research was carried out in part at the European Synchrotron Radiation Facility (ESRF). Financial support by the Fonds der chemischen Industrie (FCI) and the Bundesministerium für Bildung und Forschung (BMBF) is gratefully acknowledged.

REFERENCES CITED

Altomare, A., Burla, M.C., Camalli, M., Carrozzini, B., Cascarano, G. L., Giacovazzo, C., Guagliardi, A., Moliterni, A.G.G., Polidori, G., and Rizzi, R. (1999) EXPO:

TABLE 4. Selected geometrical data for phases I (0 GPa) and III (13.3 GPa) of Pb_3O_4 in comparison to bi- and tetravalent lead oxides and to Sr_2PbO_4

	Pb_3O_4 (13.3 GPa, 295 K)	Pb_3O_4 (0 GPa, 295 K)	β-PbO_2 (0 GPa, 295 K)	β-PbO (0 GPa, 295 K)	Sr_2PbO_4 (0 GPa, 295 K)
Distances (Å)					
Pb^{+4}-O	2.17(3) ×2	2.21 ×2	2.14 ×2		2.10 ×2
	2.21(1) ×4	2.20 ×4	2.18 ×4	–	2.27 ×4
M^{+2}-O	2.32(2) ×2	2.22 ×2	–	2.22	2.47 ×2
	2.43(2)	2.34		2.24	2.56 ×2
	2.49(2)	2.73		2.48 ↔2	2.57
	2.65(2) ×2				2.64
	2.96(2)				2.99
Pb^{+4}- M^{+2}	3.481(1)	3.79	–	–	3.63
Pb^{+4}- Pb^{+4}	3.3168(1)	3.28	3.39	–	3.50
M^{+2}- M^{+2}	3.3168(1), 3.359(2)	3.61	–	3.54	3.38, 3.50
O-O	2.81(3), 2.91(2)	2.88	2.74	2.94	2.89
Angles (°)					
O-Pb^{+4}-O	82.53(1)–98.47(1)	83.9–97.7	77.9–102.1	–	87.6–92.5
O-M^{+2}-O	66.3(4)–148.2(3)	70.6–145.3	–	48.0–151.9	70.8–150.6
Packing					
Madelung	31.02	30.08	19.03	5.82	29.88
V_1 (Å^3)*	27.8	31.8	20.8	38.5	27.3
V_2 (Å^3)†	22.7	30.2	20.0	35.9	25.4
Packing (%)	60.0	44.2	61.2	40.5	61.8
E (kJ/mol)‡	19840	19608	12354	3642	19739

Notes: The given e.s.d.'s are Rietveld statistical estimates.
* Volume per anion (normalized to zero pressure).
† Volume per anion after subtracting the volumes of the cations as calculated by MAPLE.
‡ Coulomb part of lattice energy.

a program for full powder pattern decomposition and crystal structure solution. Journal of Applied Crystallography, 32, 339–340.
Angel, R.J. (2000) Equations of State. In R.M. Hazen and R.T. Downs, Eds., High-Temperature and High-Pressure Crystal Chemistry, vol, 41, 35-60. Reviews of Mineralogy and Geochemistry, Mineralogical Society of America, Washington, D.C.
———(2002). EOSFIT, version 4.2. http://www.crystal.vt.edu/crystal/software.html.
Anderson, P.W. (1975) Model for the Electronic Structure of Amorphous Semiconductors. Physical Review Letters, 34, 953–955.
Avanesyan, V.T., Bordovskii, V.A., and Potachev, S.A. (2002) Dielectric characterization of the lone pair oxide structure. Journal of Non-Crystalline Solids, 305, 136–139.
Baur, W.H. (1972) Computer-simulated crystal structures of observed and hypothetical Mg_2SiO_4 polymorphs of low and high density. American Mineralogist, 57, 709–731.
Brauer, G. Ed. (1978) Handbuch der Präparativen Anorganischen Chemie, Ferdinand Enke Verlag Stuttgart, 3rd edition, 774–775.
Brown, I.D. (1974) Bond Valence as an aid to Understanding the Stereochemistry of O and F Complexes of Sn(II), Sb(II), Te(IV), I(V) and Cxe(XI). Journal of Solid State Chemistry, 11, 214–233.
Bystroem, A. and Westgren, A. (1943) The crystal structure of Pb_3O_4 and $SnPb_2O_4$. Arkiv foer Kemi, Mineralogi och Geologi, B16, 1–7
Chater, R., Gavarri, J.R., and Hewat, A.W. (1987), Évolution structurale sous pression de $NiSb_2O_4$: Compressibilités anisotropes et ordre magnetique. Journal of Solid State Chemistry, 67, 98–103.
Dinnebier, R.E. (1993) GUFI, a program for measurement and evaluation of powder pattern. Heidelberger Geowissenschaftliche Abhandlungen 68, XXII+332.
Finger, L.W., Cox, D.E., and Jephcoat, A.P. (1994) A correction for powder diffraction peak asymmetry due to axial divergence. Journal of Applied Crystallography, 27, 892–900.
Galy, J., Meunier, G., Andersson, S., and Åström, A. (1975) Stéréochimie des Eléments Comportant des Paires Non Liées: Ge(II), As(III), Se(IV), Br(V), Sn(II), Sb(III), Te(IV), I(V), Xe(VI), Tl(I), Pb(II), et Bi(III) (Oxydes, Fluorures et Oxyfluorures). Journal of Solid State Chemistry, 13, 142–159.
Garnier, P., Moreau, J., and Gavarri, J.R. (1990) Analyse de Rietveld de la structure de Pb(1-x) Ti(x) O(1+x) par diffraction des neutrons. Materials Research Bulletin, 25, 979–986.
Gavarri, J.R. (1982) Evolution structurale de l'oxyde isomorphes MeX_2O_4: Relation entre dilatation, vibrations et rigidite. Journal of Solid State Chemistry, 43, 12–28.
Gavarri, J.R. and Chater, R. (1989) Structural evolution, magnetic transitions, and the Gruneisen constants of the antimonites $MeSb_2O_4$. Phase Transitions, 14, 109–116.
Gavarri, J.R. and Weigel, D. (1975) Oxydes de plomb. I. structure cristalline du minium Pb_3O_4, a temperature ambiante (293 K). Journal of Solid State Chemistry, 13, 252–257.
——— (1982) Modèles Analytiques d'Evolution Structurale: Calcul des Paramètres de la Maille Orthorhombique de Pb_3O_4 en Fonction de la Température. Acta Crystallographica, A38, 195–200.
Gavarri, J.R., Weigel, D., and Hewat, A.W. (1978) Oxydes de plomb. IV. Evolution structurale de l'oxyde Pb_3O_4 entre 240 et 5 K et mecanisme de la transition. Journal of Solid State Chemistry, 23, 327–339.
Gillespie, R.J. (1967) Electron-Pair Repulsions and Molecular Shape. Angewandte Chemie, 79, 885–896; Angewandte Chemie International Edition English, 6, 819–830.
Gillespie, R.J. and Robinson, E.A. (1996) Electron- Domains and the VSEPR Model of Molecular Geometry. Angewandte Chemie, 108, 539–560; Angewandte Chemie International Edition English, 35, 495–514.
Hammersley, A.P., Svensson, S.O., Hanfland, M., Fitch, A.N., and Hausermann, D. (1996) Two-Dimensional Detector Software: From Real Detector to Idealised Image or Two-Theta Scan. High Pressure Research, 14, 235–248.
Harada, H., Sasa, Y., and Uda, M. (1981) Crystal data for beta-PbO_2. Journal of Applied Crystallography, 14, 141–142.
Hübenthal, R. (1991) MAPLE Vers. 4.0, Dissertation, University of Gießen.
Langford, J.I. and Louër, D. (1996) Powder diffraction. Reports on Progress in Physics, 59, 131–234
Larson, A.C. and Von Dreele, R.B. (1994). GSAS—General Structure Analysis System. Los Alamos National Laboratory Report LAUR 86–748.
Letoullec, R., Pinceaux, J.P., and Loubeyre, P. (1988). The membrane diamond anvil cell: A new device for generating continous pressure and temperature variation. High Pressure Research, 1, 77–90.
Mao, H.K., Xu, J., and Bell, P.M. (1986) Calibration of the ruby pressure gauge to800 kbar under quasi-hydrostatic conditions. Journal of Geophysical Research, 91, 4673–4676.
Micnas, R., Ranninger, J., and Robaszkiewicz, S. (1990) Superconductivity in narrow-band systems with local nonretarded attractive interactions. Reviews of Modern Physics, 62, 113–171.
Morimoto, N., Tokonami, M., Koto, K., and Nakajima, S. (1972) Crystal structures of the high pressure polymorphs of Mn_2GeO_4. American Mineralogist, 57, 62–75.
Robaszkiewicz, S., Micnas, R., and Ranninger, J. (1987) Superconductivity in the generalized periodic Anderson model with strong local attraction. Physical Review B36, 180–201.
Robin, M.R. and Day, P. (1970) Mixed valence chemistry—a survey and classification. In H.J. Emeleus and A.G.Sharpe, Eds., Advances in Inorganic Chemistry and Radiochemistry, vol. 10, 247–422.
Rodríguez-Carvajal, J. (2001) Recent developments of the program FULLPROF. Commission on Powder Diffraction Newsletter, 26, 12–19.
Schulze, C., Lienert, U., Hanfland, M., Lorenzen, M., and Zontone, F. (1998) Microfocusing of Hard X-rays with Cylindrically Bent Crystal Monochromators. Journal of Synchrotron Radiation, 5, 77–81.
Simon, A. (1987) Superconductivity – a Chemical Phenomenon? Angewandte Chemie, 99, 602–603; Angewandte Chemie International Edition English, 26, 579–580.
——— (1997) Superconductivity and Chemistry. Angewandte Chemie, 109, 1872–1891; Angewandte Chemie International Edition English, 36, 1788–1806.
Stephens, P.W. (1999) Phenomenological model of anisotropic peak broadening in powder diffraction. Journal of Applied Crystallography, 32, 281–289.
Terpstra, H.J., De Groot, R.A., and Haas, C. (1997) The Electronic Structure of the Mixed Valence Compound Pb_3O_4. Journal of the Physics and Chemistry of Solids, 58, 561–566.
Thompson, P., Cox, D.E., and Hastings, J.B. (1987) Rietveld refinement of Debye-Scherrer synchrotron X-ray data from Al_2O_3. Journal of Applied Crystallography, 20, 79–83.
Trömel, M. (1969), Die Kristallstruktur der Verbindungen vom Sr_2PbO_4-Typ. Zeitschrift für Anorganische und Allgemeine Chemie, 371, 237–247.
Ullmann's Encyclopedia of Industrial Chemistry, (2002) 6th edition, John Wiley and Sons, Inc.
Vinet, P., Ferrante, J., Smith, J.R., and Rose, J.H. (1986) Journal of Physics C: Solid State Physics, 19, 467–473.
Visser, J.W. (1969) A fully automatic program for finding the unit cell from powder data. Journal of Applied Crystallography, 2, 89–95.
Wadsley, A.D., Reid, A.F., and Ringwood, A.E. (1968) The high-pressure form of Mn_2GeO_4, a member of the olivine group. Acta Crystallographica, B24, 740–742.

MANUSCRIPT RECEIVED NOVEMBER 12, 2002
MANUSCRIPT ACCEPTED JANUARY 13, 2003
MANUSCRIPT HANDLED BY MICHAEL FECHTELKORD